Spectroscopy of a deterministic single-donor device in silicon

M. Fuechsle[*a], J. A. Miwa[a], S. Mahapatra[a], H. Ryu[b], S. Lee[b], O. Warschkow[c], L. C. L. Hollenberg[d], G. Klimeck[b], and M. Y. Simmons[a]

[a]Centre for Quantum Computation & Communication Technology, University of New South Wales, Sydney, NSW 2052, Australia; [b]Network for Computational Nanotechnology, Birck Nanotechnology Center, Purdue University, West Lafayette, Indiana 47907, USA; [c]Centre for Quantum Computation & Communication Technology, University of Sydney, Sydney, NSW 2006, Australia; [d]Centre for Quantum Computation & Communication Technology, University of Melbourne, VIC 3010, Australia

ABSTRACT

We present a single electron transistor (SET) based on an individual phosphorus dopant atom in an epitaxial silicon environment. Using scanning tunneling microscope (STM) hydrogen lithography, the single impurity is deterministically placed with a spatial accuracy of ±1 lattice site within a donor-based transport device. Low temperature transport measurements confirm the presence of the single donor and show that the donor charge state can be precisely controlled via gate voltages. We observe a charging energy that is remarkably similar to the value expected for isolated P donors in bulk silicon, which is in sharp contrast to previous experiments on single-dopant transport devices. We show that atomistic modeling can fully capture the effects of the highly-doped transport electrodes on the electronic states of the donor, thus highlighting the high level of control over the electrostatic device properties afforded by a deterministic single donor architecture. Our fabrication method therefore opens the door for the realization of a scalable donor-based qubit architecture in silicon.

Keywords: Silicon, Quantum Computation, Scanning Tunneling Microscopy (STM), STM lithography, Single-atom devices

1. INTRODUCTION

The spin states associated with donors in silicon are a promising candidate for the realization of quantum logic devices due to their resilience against decoherence[1-2]. This is essentially due to two desirable material properties of silicon,[3] the predominance of spin-zero ^{28}Si nuclei and a small spin-orbit coupling. As a result, various silicon-based quantum computer architectures have been proposed, using either the nuclear spin,[3] or donor electron spin[4] or charge[5] of individual phosphorus dopants to define the qubit. Furthermore, nuclear spins of ^{31}P in a silicon-environment have also been demonstrated to serve as suitable quantum memory for spin superposition states[6] with a lifetime exceeding 100 s.[7] However, while considerable progress has recently been made towards spin manipulation and spin read-out,[8] a remaining challenge is the scale-up of donor-based quantum information devices. While proposals exist for scalable two-dimensional architectures,[9] these rely on vast arrays of individual impurities. To avoid spatial oscillations in the exchange coupling between neighboring donor sites arising from the silicon bandstructure,[10] these architectures require precise control over the location of each dopant atom within the array. A key challenge in fabricating a functional donor-based qubit is therefore the ability to pattern individual impurities in an epitaxial silicon environment with essentially atomic accuracy.

Here, we demonstrate how STM hydrogen lithography can be used as a viable tool to overcome this challenge since it allows individual dopants to be patterned within a functional transport structure with a spatial accuracy of one lattice site.

[*] martin.fuechsle@unsw.edu.au; michelle.simmons@unsw.edu.au; www.cqc2t.org

Quantum Information and Computation X, edited by Eric Donkor, Andrew R. Pirich, Howard E. Brandt,
Proc. of SPIE Vol. 8400, 840006 · © 2012 SPIE · CCC code: 0277-786X/12/$18 · doi: 10.1117/12.919763

2. FABRICATION

One of the key advantages of using STM for device fabrication is that it can be turned from a surface patterning tool into a non-invasive imaging tool simply by adjusting the tip voltage and tunneling current. This allows us to image the structure at every step of the patterning process. Fig. 1a illustrates the fabrication of the dopant-based transport structure. Here, the 3D perspective representation shows an STM image of the hydrogen (H) terminated Si(100) surface where the STM tip has been used to selectively desorb a four-terminal structure. In a subsequent step, these regions will be dosed with phosphine (PH_3) to form phosphorus-doped co-planar transport electrodes where the dopants are essentially confined to a single atomic plane in growth (*z*-) direction. Due to the high doping density (corresponding to a sheet coverage of ~ 0.25 monolayers), the STM-patterned regions will conduct down to cryogenic temperatures while the surrounding substrate becomes insulating due to the freeze-out of mobile carriers. This fabrication method has previously enabled the fabrication of planar dopant-based quantum dot structures both in the many-electron regime[11] as well as in the few-donor regime.[12] Fig. 1b is a close-up of the inner device region showing the source (S) and drain (D) leads which are precisely aligned to a single phosphorus donor that has been incorporated in the center of the device (indicated by the white rectangle). Two in-plane gates (G1 and G2) are patterned on either side of the S-D transport channel to control the electrostatic potential at the position of the donor. The gates are patterned further away (at a distance of 54 nm from the donor site) to avoid gate leakage currents from direct tunneling to the leads.

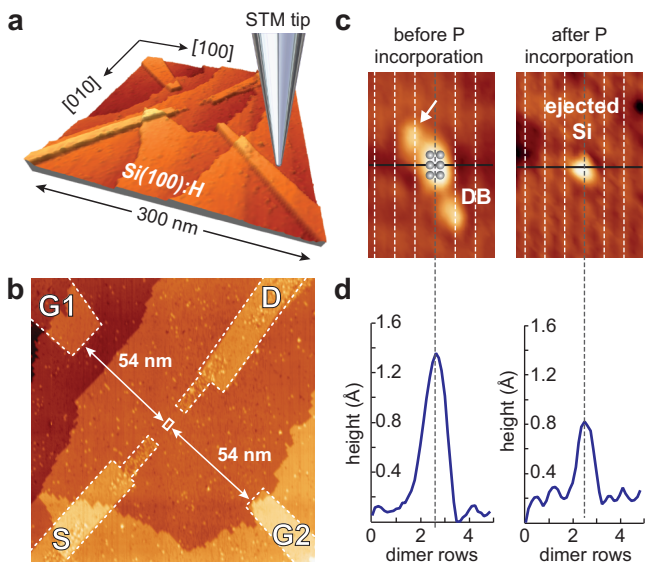

Figure 1. a) Illustration of STM lithography on a hydrogen terminated Si(100) surface. Several atomic steps are visible on the surface. The regions where the H layer has been desorbed with the STM tip appear raised in the perspective STM image. b) STM image of the inner device region showing the H-desorbed regions (outlined for clarity) which define the source (S) and drain (D) leads as well as two in-plane gates (G1 and G2). A close-up of the designated single donor incorporation site (indicated by the solid white rectangle) is shown in (c), both before (left panel) and after (right panel) the phosphine dosing and incorporation anneal cycle. Vertical dashed lines indicate dimer rows. The superimposed grey circles in the left panel indicate the 6 bare Si sites. The two additional features are due to a single dangling bond (DB) and a tip-related imaging artifact (white arrow), respectively. The incorporation reaction is further evidenced by a distinctive change in the apparent height profiles of the observed surface features , from 1.4 ± 0.2 Å to 0.8 ± 0.1 Å d, depicted in (d).

The fabrication is achieved in a two-step process. First, the intended incorporation area for the central single donor is desorbed along with the innermost parts of the leads. After an initial PH_3 dosing and incorporation anneal cycle, the area

is imaged again to verify the successful incorporation of a single P. Next, the in-plane gates are aligned and desorbed along with the extensions of the leads as shown in Fig. 1b. The incorporation pathway from the adsorbed phosphine molecules on the bare Si surface to the incorporated P donors is well-understood[13-15] and occurs as a sequence of dissociative processes: The chemisorbed PH_3 successively loses all 3 H atoms to neighboring bare Si sites until the remaining P adatom (upon thermal activation) incorporates into the Si surface, ejecting a silicon adatom in the process. Further details of the fabrication are discussed in Ref. 16. Importantly, we find that 3 adjacent dimers (i.e. pairs of Si surface atoms) along one dimer row are necessary to incorporate precisely one P atom, in agreement with theoretical predictions[14] as well as previous incorporation experiments.[17] A high-resolution image of the designated single donor incorporation site is shown in Fig. 1c, both before (left panel) and after (righ panel) the dosing and incorporation anneal cycle. In the left panel, we can clearly identify the 6 H-desorbed bare Si sites. Upon dosing with of PH_3 and a short incorporation anneal at 350 ºC, we observe a clear change in the surface morphology along with different height profiles of the surface features (Fig. 1d). In the right panel of Fig. 1c, the successful incorporation of a single P donor is evidenced by the observation of a single Si adatom which appears as a bright protrusion centered on a dimer row.[18] Since the incorporated P atom substitutes for one of the 6 Si atoms within the 3-dimer site, the lateral spatial patterning accuracy of our method corresponds to ± 1 Si lattice site (± 3.8 Å).

After the subsequent H-desorption of the transport electrodes and the second dosing and incorporation anneal cycle, the entire device is overgrown with ~ 180 nm epitaxial silicon. The low growth temperature of 250 ºC maintains the structural integrity of the Si:P structure and minimizes dopant segregation.[19] In a last step, *ex-situ* metallic leads are defined over the STM-patterned dopant regions to form ohmic contacts.

3. MEASUREMENTS

The transport properties of our single donor device were characterized in a $^3He/^4He$ dilution refrigerator at base temperature (~ 20 mK). In this temperature regime, the frozen-out intervening silicon substrate constitutes a tunnel barrier between the electrodes and electronic transport from S to D occurs via the discrete donor states. Fig. 2b shows the measured gate leakage current for both gates (flowing from each gate to any of the other electrodes) as a function of the applied gate voltage. We find that the available gate range is smaller for the narrower gate, G2. This is possibly due to a higher potential gradient around the tip of a narrow electrode which results in a smaller effective tunnel barrier. The leakage curves for both gates are asymmetric for positive and negative gate voltages with a significantly higher break-through voltage for $V_G > 0$. This is consistent with findings from previous donor-based quantum dot devices[11-12] and may result from partial depletion of the gate electrodes for large positive voltages.[11]

In Fig. 2a, the dc source-drain current I_{SD} is plotted as a function of the bias voltage V_{SD} and gate voltage V_G (applied to gates G1 and G2 in parallel). In this so-called stability diagram, the current is suppressed in the diamond-shaped white regions due to Coulomb blockade. We find that the 'diamond' for $V_G \leq 450$ mV does not close, i.e. the blockaded bias region increases nearly linearly with decreasing gate voltage all the way down to the lower end of the gate range. This behavior is indicative[20] of the positively ionized D^+ state of a single P donor which cannot lose more that its one valence electron. We thus identify the two other charge-stable regions in Fig. 2a as the charge-neutral D^0 state (450 mV < V_G < 820 mV) and the two-electron D^- state (V_G > 820 mV) of the donor, respectively. This identification can be further confirmed by measuring the gate voltage spacing ΔV_G between the two Coulomb peaks (corresponding to the D^+/D^0 and D^0/D^- charge transitions, respectively) as a function of an applied magnetic field B (Fig. 2c). A magnetic field breaks the spin degeneracy of the donor states, splitting the spin-up and spin-down states by the Zeeman energy[21] $E_Z = \Delta s_z g \mu_B B$. Here, g is the electron g-factor, μ_B is the Bohr magneton, and $\Delta s_z = \pm ½$ is the total change in spin momentum associated with a charge transition. For the D^0 state, the one bound electron spin aligns with the external B-field so that the D^+/D^0 transition is lowered in energy and thus shifts down in gate voltage. Conversely, the D^0/D^- transition is shifted up in energy. The spacing ΔV_G between the two Coulomb peaks therefore increases with $g\mu_B B$. Indeed, we observe the expected increase of ΔV_G, as illustrated in Fig. 2c. A linear fit (indicated by the red line) yields a slope of ~ 1.17 mV/T. Using the gate coupling factor $\alpha = E_C / \Delta V_G \approx 0.1$ extracted from Fig. 2a we can convert the measured slope into an energy shift of 117 μeV/T from which we can determine an experimental value for the g-factor of ~ 2.0, in excellent agreement with the expected value (g = 2.0)[22] for electrons in silicon.

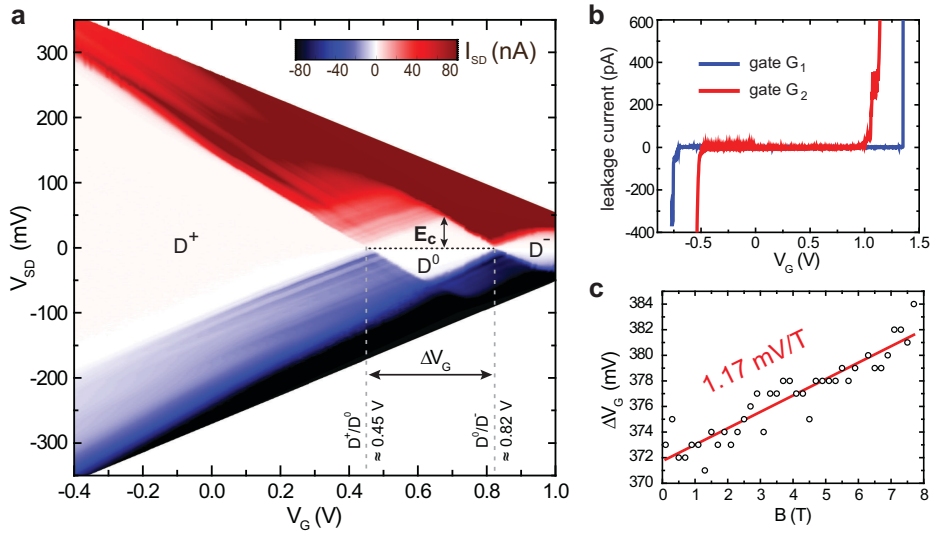

Figure 2. a) Stability diagram of a single P donor at milliKelvin temperatures. The source-drain current I_{SD} is plotted as a function of bias voltage V_{SD} and gate voltage V_G (applied to both gates in parallel). The height of the D^0 diamond yields a charging energy $E_C = 47 \pm 3$ meV. At zero gate voltage, the donor is in the ionized D^+ state. b) The measured gate leakage currents as a function of the applied gate voltage define the available gate range for each gate. c) The gate voltage spacing ΔV_G between the two charge transitions in (a) as a function of the magnetic field B. To extract the values for ΔV_G, the gate voltage was swept continuously at a constant bias (V_{SD} = 100 μV) while B was increased in 200 mT increments.

The charging energy E_C for our single-donor transport device can be directly determined from the height of the D^0 diamond in Fig. 2a, for which we obtain $E_C = 47 \pm 3$ meV. This charging energy is remarkably similar to the value of ~ 44 meV that one would expect for an isolated P donor in bulk silicon, considering the binding energies (45.6 meV for D^0 and ~ 1.7 meV for the two-electron state D^-, respectively)[23] determined by absorption spectroscopy experiments. This bulk-like charging energy is in sharp contrast to previously reported single dopant transport experiments in silicon.[20,24-25] There, the measured E_C was either found to be significantly reduced compared to the corresponding bulk value due to screening effects arising from strong capacitive coupling of the dopant to a nearby gate[20] or strong electric fields,[25] while other experiments found charging energies exceeding the bulk value due to an increased donor ionization energy in the proximity of a dielectric interface.[24] In our transport device, however, it is plausible that these effects are small since i) the electric field at the position of the donor is negligible due to the symmetric layout of the two gates and ii) the device is encapsulated deep within an epitaxial silicon environment so that the donor is far away from any heterogeneous interfaces.

It may at first be surprising in Fig. 2a that the donor is *not* its charge-neutral state at zero gate voltage, as would be expected for an isolated bulk donor at milliKelvin temperatures. Indeed, the D^+/D^0 charge transition in our device reproducibly occurs at a finite positive gate voltage of 450 ± 30 mV. Importantly, this behaviour is consistent even between different cool-downs of the device and is not due to offset charges. Instead, the electrostatic characteristics reflect the inherent influence of the nearby highly-doped leads within our transport device where the conductance depends on the relative detuning of the donor eigenstates with respect to the Fermi level in the leads.

4. DEVICE MODELING

This detuning can be calculated as a function of the applied gate voltage using a multi-scale modeling approach to describe our donor-based structure.[16,26] Since the device is too large to be treated atomistically as a whole, we first compute the potential landscape self-consistently between the four transport electrodes using a Thomas-Fermi approximation. This is illustrated in Fig. 3a, where the superimposed Coulombic potential represents the central P donor

core. In contrast to an isolated impurity in bulk silicon, the donor potential in our device is anisotropic since the proximity of the highly-doped leads effectively lowers the potential along the S-D transport direction. The eigenstates are then calculated for this modified donor potential using an atomistic tight-binding approach implemented in the NEMO-3D (Nanoelectronic Modeling tool)[27] simulator. The position of the D^0 state for $V_G = 0$ (solid red line) is shown in Fig. 3b along with a linecut through the potential profile along S-D (solid blue line) which defines the tunnel barriers between the leads. Both lines are plotted with respect to the Fermi level E_F in the leads which is obtained from a separate atomistic calculation of the dopant nanowires[28] defining the electrodes. At $V_G = 0$, the calculated D^0 state is indeed found to reside ~ 80 meV above E_F so that it cannot contribute to transport through the device at low bias.

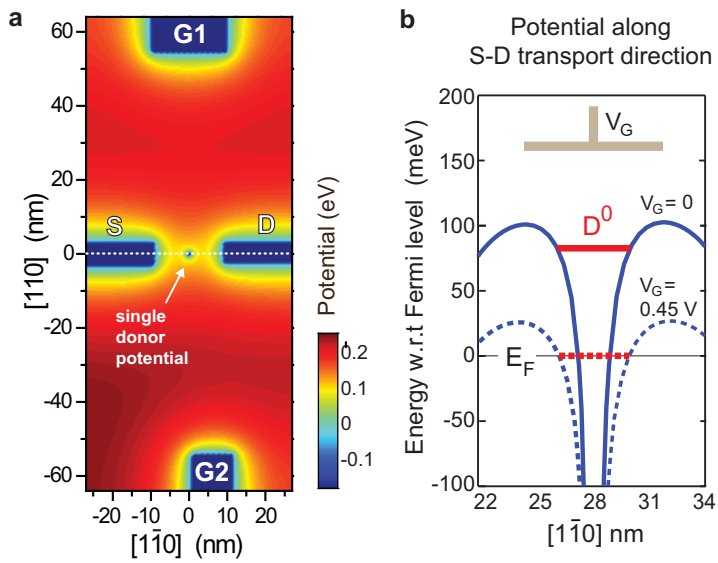

Figure 3. a) False-color plot showing the potential landscape calculated for the inner device region at $V_G = V_{SD} = 0$. The domain size for the Thomas-Fermi calculation was 56 nm x 128 nm in the lateral direction, and 180 nm in z- (growth) direction on either side of the dopant plane. The superimposed Coulombic potential in the center represents the single P donor. The proximity of the highly-doped leads results in a lower effective potential between the S and D electrodes. b) Linecut of the potential profile along the S-D transport direction, indicated by the white dashed line in (a). By applying a gate voltage $V_G > 0$, the donor eigenstates can be shifted down. At $V_G = 0.45$ V (dashed lines) the D^0 state comes into resonance with the leads, so that current can flow through the device.

However, by applying a positive voltage to the in-plane gates (schematically indicated in Fig. 3b) the donor states can be shifted towards lower energies. At $V_G = 0.45$ V, the one-electron groundstate D^0 is aligned with the Fermi level in the leads, as depicted in Fig. 3b. At the same time, the barrier height is significantly reduced compared to the equilibrium case at $V_G = 0$. This is due to the non-proximal coupling of the gates, where the applied gate voltage not only shifts the electrochemical potential of the donor states, but also modulates the potential landscape between the leads.

The calculated transition gate voltage is in excellent agreement with the transport data where the transition between the D^+ and D^0 regions occurs at the same value of V_G (Fig. 2a). At this point, the Coulomb blockade of the device is lifted so that electrons can tunnel from S to D even at low bias voltages. For gate voltages > 0.45 V, conductance is again blocked and the device is in a charge-stable configuration with one electron bound to the donor. This can be accounted for by self-consistently filling the initial Coulomb potential with one electron which effectively screens the donor core potential. The resulting D^- state is therefore higher in energy (and thus weaker bound). This two-electron ground state can again be shifted down in energy by further increasing the gate voltage until it eventually crosses E_F at $V_G = 0.72$ V, which is in reasonable agreement with the experimental value of 0.82 V for the second charge transition (Fig. 2a). The charging energy of our model is given by the energy difference between the calculated D^0 and D^- states, for which we obtain a value of 46.5 meV. The slight deviation between the calculated value and the ~ 44 meV expected for the bulk

case[23] most likely arises from the artificial confinement defined by the boundaries of the simulation domain used for the atomistic calculations.[16]

5. CONCLUSIONS

We have demonstrated the fabrication of a deterministic single-donor device in silicon, where an individual phosphorus atom is deterministically placed with sub-nm scale accuracy between dopant-based transport electrodes. The remarkable agreement between our multi-scale modeling approach and the experimental observations – both in terms of the charge transition points as well as the charging energy – is testament to the high level of control over the electrostatic device properties afforded by our atomically precise fabrication method. In particular, the calculations fully support the bulk-like charging energy measured in our single-donor device which we attribute to the absence of nearby metallic gates or interfaces and the vanishing gate electric field afforded by our device design. The fabrication technique presented here opens the door for novel device concepts which use single dopant atoms as their active elements. In particular, our work presents an important step towards the realization of a scalable donor-based qubit architecture.

ACKNOWLEDGEMENTS

The authors acknowledge discussions with S. Rogge, J. Verduijn and R. Rahman. This research was conducted by the Australian Research Council Centre of Excellence for Quantum Computation and Communication Technology (project no. CE110001027). The research was also supported by the US National Security Agency and the US Army Research Office (contract no. W911NF-08-1-0527). L.H. acknowledges an Australian Professorial Fellowship. M.Y.S. acknowledges a Federation Fellowship.

REFERENCES

[1] Feher, G., "Electron spin resonance experiments on donors in silicon. 1. Electronic structure of donors by the electron nuclear double resonance technique," *Phys. Rev.* 114(5), 1219-1244 (1959).

[2] Tyryshkin, A. M., Lyon, S. A., Astashkin, A. V. and Raitsimring, A. M., "Electron spin relaxation times of phosphorus donors in silicon," *Phys. Rev. B* 68(19), 193207 (2003).

[3] Kane, B. E., "A silicon-based nuclear spin quantum computer" *Nature* 393(6681), 133-137 (1998).

[4] Vrijen, R., Yablonovitch, E., Wang, K., Jiang, H. W., Balandin, A., Roychowdhury, V., Mor, T. and DiVincenzo, D., "Electron-spin-resonance transistors for quantum computing in silicon-germanium heterostructures," *Phys. Rev. A* 62(1), art. no.-012306 (2000).

[5] Hollenberg, L. C. L., Dzurak, A. S., Wellard, C., Hamilton, A. R., Reilly, D. J., Milburn, G. J. and Clark, R. G., "Charge-based quantum computing using single donors in semiconductors," *Phys. Rev. B* 69(11), 4 (2004).

[6] Morton, J. J. L., Tyryshkin, A. M., Brown, R. M., Shankar, S., Lovett, B. W., Ardavan, A., Schenkel, T., Haller, E. E., Ager, J. W. and Lyon, S. A., "Solid-state quantum memory using the ^{31}P nuclear spin," *Nature* 455(7216), 1085-1088 (2008).

[7] McCamey, D. R., Van Tol, J., Morley, G. W. and Boehme, C., "Electronic spin storage in an electrically readable nuclear spin memory with a lifetime > 100 seconds," *Science* 330(6011), 1652-1656 (2010).

[8] Morello, A., Pla, J. J., Zwanenburg, F. A., Chan, K. W., Tan, K. Y., Huebl, H., Mottonen, M., Nugroho, C. D., Yang, C. Y., van Donkelaar, J. A., Alves, A. D. C., Jamieson, D. N., Escott, C. C., Hollenberg, L. C. L., Clark, R. G. and Dzurak, A. S., "Single-shot readout of an electron spin in silicon," *Nature* 467(7316), 687-691 (2010).

[9] Hollenberg, L. C. L., Greentree, A. D., Fowler, A. G. and Wellard, C. J., "Two-dimensional architectures for donor-based quantum computing," *Phys. Rev. B* 74(4), 045311 (2006).

[10] Koiller, B., Hu, X. D. and Das Sarma, S., "Exchange in silicon-based quantum computer architecture," *Phys. Rev. Lett.* 88(2), 027903 (2002).

[11] Fuhrer, A., Fuchsle, M., Reusch, T. C. G., Weber, B. and Simmons, M. Y., "Atomic-Scale, All Epitaxial In-Plane Gated Donor Quantum Dot in Silicon," *Nano Lett.* 9(2), 707-710 (2009).

[12] Fuechsle, M., Mahapatra, S., Zwanenburg, F. A., Friesen, M., Eriksson, M. A. and Simmons, M. Y., "Spectroscopy of few-electron single-crystal silicon quantum dots," *Nat. Nanotechnol.* 5(7), 502-505 (2010).

[13] Wilson, H. F., Warschkow, O., Marks, N. A., Schofield, S. R., Curson, N. J., Smith, P. V., Radny, M. W., McKenzie, D. R. and Simmons, M. Y., "Phosphine dissociation on the Si(001) surface," *Phys. Rev. Lett*. 93(22), 4 (2004).

[14] Wilson, H. F., Warschkow, O., Marks, N. A., Curson, N. J., Schofield, S. R., Reusch, T. C. G., Radny, M. W., Smith, P. V., McKenzie, D. R. and Simmons, M. Y., "Thermal dissociation and desorption of PH3 on Si(001): A reinterpretation of spectroscopic data," *Phys. Rev. B* 74(19), 195310 (2006).

[15] Warschkow, O., Wilson, H. F., Marks, N. A., Schofield, S. R., Curson, N. J., Smith, P. V., Radny, M. W., McKenzie, D. R. and Simmons, M. Y., "Phosphine adsorption and dissociation on the Si(001) surface: An ab initio survey of structures," *Phys. Rev. B* 72(12), 125328 (2005).

[16] Fuechsle, M., Miwa, J. A., Mahapatra, S., Ryu, H., Lee, S., Warschkow, O., Hollenberg, L. C. L., Klimeck, G. and Simmons, M. Y., "A single-atom transistor," *Nature Nanotechnol*. DOI: 10.1038/NNANO.2012.21 (2012).

[17] Schofield, S. R., Curson, N. J., Simmons, M. Y., Ruess, F. J., Hallam, T., Oberbeck, L. and Clark, R. G., "Atomically precise placement of single dopants in Si," *Phys. Rev. Lett.* 91(13), 136104 (2003).

[18] Brocks, G., Kelly, P. J. and Car, R., "The energetics of adatoms on the Si(100) surface," *Surf. Sci.* 269, 860-866 (1992).

[19] Oberbeck, L., Curson, N. J., Hallam, T., Simmons, M. Y., Bilger, G. and Clark, R. G., "Measurement of phosphorus segregation in silicon at the atomic scale using scanning tunneling microscopy," *Appl. Phys. Lett.* 85(8), 1359-1361 (2004).

[20] Lansbergen, G. P., Rahman, R., Wellard, C. J., Woo, I., Caro, J., Collaert, N., Biesemans, S., Klimeck, G., Hollenberg, L. C. L. and Rogge, S., "Gate-induced quantum-confinement transition of a single dopant atom in a silicon FinFET," *Nat. Phys.* 4(8), 656-661 (2008).

[21] Hanson, R., Kouwenhoven, L. P., Petta, J. R., Tarucha, S. and Vandersypen, L. M. K., "Spins in few-electron quantum dots,," *Rev. Mod. Phys.* 79(4), 1217-1265 (2007).

[22] Young, C. F., Poindexter, E. H., Gerardi, G. J., Warren, W. L. and Keeble, D. J., "Electron paramagnetic resonance of conduction-band electrons in silicon," *Phys. Rev. B* 55(24), 16245-16248 (1997).

[23] Ramdas, A. K. and Rodriguez, S., "Spectroscopy of the solid-state analogs of the hydrogen atom: donors and acceptors in semiconductors," *Rep. Prog. Phys.* 44(12), 1297-1387 (1981).

[24] Pierre, M., Wacquez, R., Jehl, X., Sanquer, M., Vinet, M. and Cueto, O., "Single-donor ionization energies in a nanoscale CMOS channel," *Nat. Nanotechnol.* 5(2), 133-137 (2010).

[25] Rahman, R., Lansbergen, G. P., Verduijn, J., Tettamanzi, G. C., Park, S. H., Collaert, N., Biesemans, S., Klimeck, G., Hollenberg, L. C. L. and Rogge, S., "Electric field reduced charging energies and two-electron bound excited states of single donors in silicon," *Phys. Rev. B* 84(11), 115428 (2011).

[26] Ryu, H., Lee, S., Tan, Y. H., Klimeck, G., Fuechsle, M., Miwa, J. A., Mahapatra, S., Simmons, M. Y. and Hollenberg, L. C. L., "Toward single atom transistors: A tight-binding study on single donor quantum dots," *to be submitted.*

[27] Klimeck, G., Oyafuso, F., Boykin, T. B., Bowen, R. C. and von Allmen, P., "Development of a nanoelectronic 3-D (NEMO 3-D) simulator for multimillion atom simulations and its application to alloyed quantum dots," *CMES-Comp. Model. Eng. Sci*. 3(5), 601-642 (2002).

[28] Weber, B., Mahapatra, S., Ryu, H., Lee, S., Fuhrer, A., Reusch, T. C. G., Thompson, D. L., Lee, W. C. T., Klimeck, G., Hollenberg, L. C. L. and Simmons, M. Y., "Ohm's Law Survives to the Atomic Scale," *Science* 335(6064), 64-67 (2012).